JOURNAL OF AIRCRAFT
Vol. 42, No. 4, July–August 2005

Joined-Wing Aeroelastic Design with Geometric Nonlinearity

Maxwell Blair*
U.S. Air Force Research Laboratory, Wright–Patterson Air Force Base, Ohio 45433-7542
Robert A. Canfield†
Air Force Institute of Technology, Wright–Patterson Air Force Base, Ohio 45433-7765
and
Ronald W. Roberts Jr.‡
U.S. Air Force Research Laboratory, Wright–Patterson Air Force Base, Ohio 45431-7542

An integrated process is presented that advances the design of an aeroelastic joined-wing concept by incorporating physics-based results at the system level. For instance, this process replaces empirical mass estimation with high-fidelity analytical mass estimations. Elements of nonlinear structures, aerodynamics, and aeroelastic analyses were incorporated with vehicle configuration design. This process represents a significantly complex application of aeroelastic structural optimization. Specific fuel consumption for a fixed lift-to-drag ratio was considered in the process for estimating fuel to size the structure to meet range and loiter requirements. This design process was implemented on a single configuration for which two crucial nonlinear phenomena contribute to structural failure: large deformation aerodynamics and geometrically nonlinear structures. A correct model of the nonlinear aeroelastic physics offers the possibility of a successful design. Unconventional features of a joined-wing concept are presented with the aid of this unique design model. Hopefully, insight derived from the nonlinear aeroelastic design might be leveraged to the benefit of future joined-wing designs.

Nomenclature

C	=	specific fuel consumption
c	=	wing chord
d	=	effective wing depth
L/D	=	lift-to-drag ratio
L/H	=	fuselage fineness ratio (length/height)
q	=	dynamic pressure
R_i	=	range of the vehicle over ith mission segment
V	=	vehicle velocity
W_F	=	fuselage structural weight
W_{IE}	=	installed engine weight
W_i	=	vehicle weight in ith mission segment
W_{to}	=	vehicle weight at takeoff
W_{UE}	=	uninstalled engine weight
x_{fa}	=	aft wing offset along fuselage axis
z_{fa}	=	aft wing offset in vertical direction

I. Introduction

THE joined-wing (Fig. 1) is a radical departure from the world's inventory of aircraft. The target application for this study is an airborne sensor mission. Optimizing structural mass in support of this mission holds out the possibility that the joined-wing concept may still offer mass savings where structural stiffness is a design constraint. If so, geometric nonlinearity and associated aeroelastic interactions will play a primary role. The results presented here build on significant prior work.

Received 1 May 2003; presented as Paper US-5 at the IFASD—International Forum on Aeroelasticity and Structural Dynamics, Amsterdam, NL, 4 June 2003; revision received 1 March 2005; accepted for publication 10 December 2004. This material is declared a work of the U.S. Government and is not subject to copyright protection in the United States. Copies of this paper may be made for personal or internal use, on condition that the copier pay the $10.00 per-copy fee to the Copyright Clearance Center, Inc., 222 Rosewood Drive, Danvers, MA 01923; include the code 0021-8669/05 $10.00 in correspondence with the CCC.

*Research Engineer, Air Vehicles Directorate; maxwell.blair@wpafb.af.mil. Associate Fellow AIAA.
†Associate Professor, Department of Aeronautics and Astronautics; robert.canfield@afit.edu. Associate Fellow AIAA.
‡Structural Composites Research Engineer, Materials and Manufacturing Directorate; ronald.roberts@wpafb.af.mil.

The joined-wing concept has been studied by a number of designers and specialists since 1986 when Wolkovich[1] published his concept. Hajela and Chen published preliminary findings regarding finite element method (FEM) based mass estimation of a joined-wing concept.[2] Livne has provided a valuable survey paper on these technical developments.[3] Gallman and Kroo[4] offered many recommendations, including the use of fully stressed design (FSD) optimization criteria and nonlinear analysis. These authors showed that the joined-wing configuration in that study was actually heavier than a conventional commercial transport airplane, thereby deflating interest in joined-wing technology. However, they did hold out the possibility that joined-wing designs may be advantageous in the context of other missions.

Blair and Canfield[5] initiated nonlinear exploration on a joined-wing configuration with approximately twice the span of Gallman and Kroo's model. The current effort continues with the development of a joined-wing design model integrated with automated aerodynamic and structures assessments in a single environment. Preliminary results from the current study were first presented in Ref. 6.

Complementing the work presented here is the work of Weisshaar and Lee,[7] who provided significant insight into the important role of flutter in constraining joined-wing design. Their models included structural optimization of laminated composite material with linear static aeroelastic and flutter constraints.

A tailored design environment forms the basis for computational design studies. Wakayama studied an innovative blended wing–body concept[8] using a common environment for physics-based modeling. Samareh and Bhatia[9] developed a unifying approach for multidisciplinary design at the vehicle level. Surface geometry was structured to serve as a unifying medium, with the benefit that this saves on data storage where a number of disciplines interact.

The high-altitude long-endurance (HALE) mission calls for a very large wingspan, resulting in greater flexibility than more conventional aircraft wings. This alone invites a reexamination of the joined-wing concept. The joined-wing concept is revisited as a mass-competitive alternative with the development of nonlinear analysis and design tools. Conventional wisdom suggests trading drag reduction (through decreased airfoil thickness for transonic flight) with mass reduction (associated with increased wing box depth for structural efficiency). Maintaining dynamic pressure at higher altitudes requires increased speed, ultimately leading to transonic effects during cruise and loiter. Conventional wisdom should be reexamined

in light of the joined-wing's potential for structurally efficient wing boxes enclosed within thin airfoil sections.

Some have compared the joined-wing and the strut-braced wing (SBW) concepts. Indeed, one could develop a design study with a continuous spectrum of shapes ranging from a joined wing to an SBW. In both cases, the primary wing is reinforced with a second structure, thus introducing structural members with predominately compressive loads. Recent studies[10] indicate the SBW may be a superior design over traditional cantilever wing designs for transonic commercial operations. However, it is the airborne sensor mission that drives this study of a joined-wing vehicle.

In the final analysis, the optimal design objective will involve a combination of sensor performance, aerodynamic performance, and mass. The goal of the current effort is to combine structural sizing for a moderately high-fidelity FEM to converge on a configuration that simultaneously satisfies the following: 1) aerodynamic performance requirements with respect to range and loiter, 2) equilibrium of integrated aerodynamic and gravity forces in pitch and lift, and 3) structural stress in static aeroelastic equilibrium.

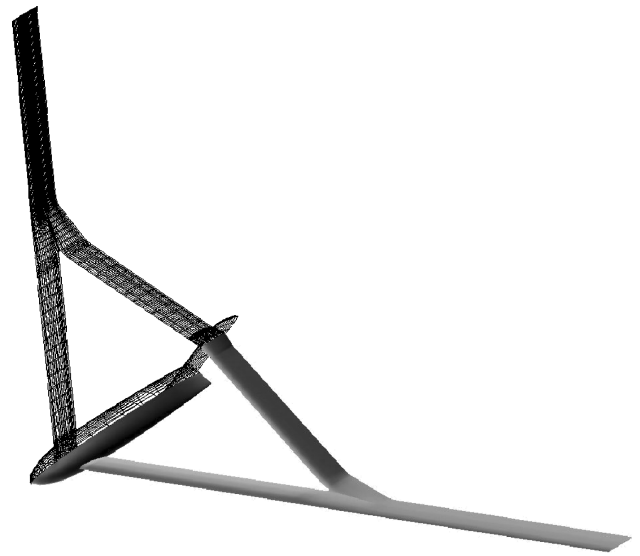

Fig. 1 Joined-wing configuration.

The traditionally held challenge for a joined-wing design has been to identify and overcome the nonlinear buckling response of the aft wing. The high-fidelity model presented here has demonstrated that the front wing can also buckle. In either case, as the joined-wing structure is resized and buckling becomes critical, it is necessary to account for stresses arising from large nonlinear deformations. Of course, this introduces a serious complication into the preliminary design process.

This paper covers a wide range of perspectives, all of which contribute to the final optimized joined-wing vehicle design. It begins with a description of the joined-wing vehicle and variable geometric entities (software objects). The next section provides a top-level description of the design environment. The following sections address the modeling methods integrated for aerodynamic, structural, and aeroelastic analyses, respectively. An overview of the design processes employed follows. This precedes the section that focuses on a description of the baseline model. The final section presents the optimized results for the trimmed linear and nonlinear aeroelastic vehicle.

II. Joined-Wing Vehicle

A. Vehicle Geometric Variables

The configuration is driven by a significant number of parameters, some of which are listed in Table 1, for the baseline. A generic schematic is provided in Fig. 2 to help interpret these parameters.

Table 1 Configuration parameters with baseline values

Parameter	Symbol	Value
Inboard span, m	S_{ib}	26.00
Outboard span, m	S_{ob}	8.00
Fore root chord, m	c_{rf}	2.50
Aft root chord, m	c_{ra}	2.50
Midchord, m	c_m	2.50
Tip chord, m	c_t	2.50
Fore–aft x offset, m	x_{fa}	19.50
Fore–aft z offset, m	z_{fa}	7.00
Inboard sweep, deg	Λ_{ib}	30
Outboard sweep, deg	Λ_{ob}	30
Airfoil		LRN-1015
Calculated wing planform area, m^2	S	143.5
Calculated wing volume, m^3		71.7

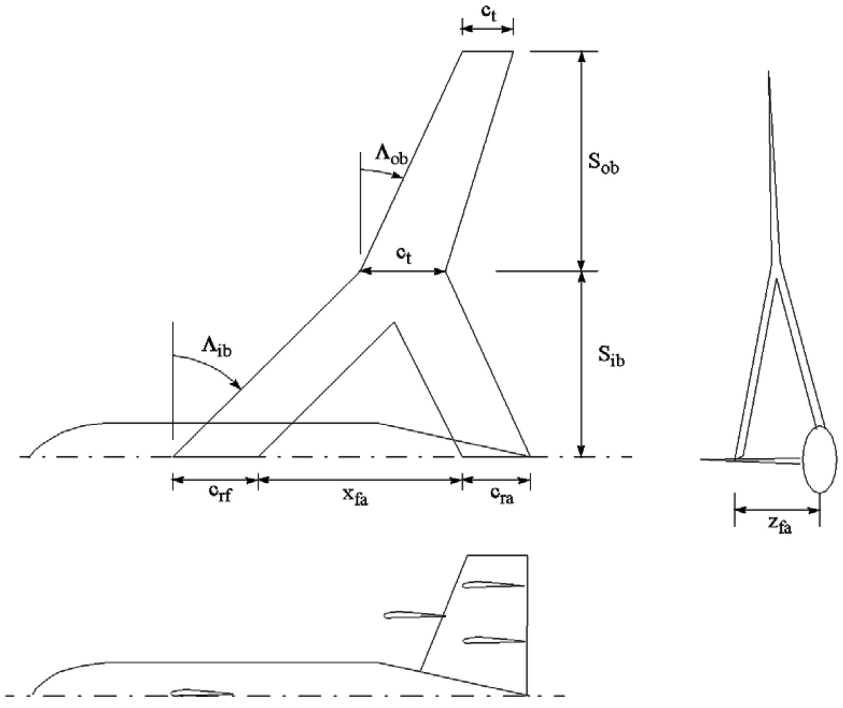

Fig. 2 Planform configuration.

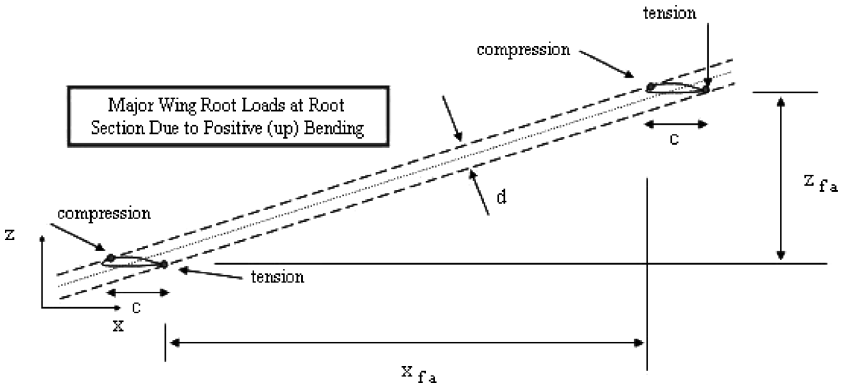

Fig. 3a Minimum wing root bending axis.

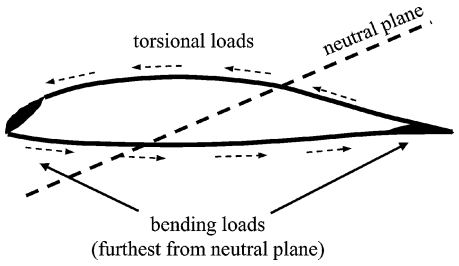

Fig. 3b Simplified loads on idealized section.

(Note that with these parameters, we have the potential to transform from a joined-wing configuration to an SBW.)

B. Wing Thickness

In Fig. 3a, the effective wing depth d increases with greater vertical offset of the aft wing z_{fa}, and chord c and less horizontal offset of the wing roots x_{fa},

$$d = c(z_{fa}/x_{fa}) \tag{1}$$

Thus, this leads the structural designer to advocate increased z_{fa} and c and decreased x_{fa} to increase system stiffness. Conventional design rules associate aerodynamically thick airfoils with structurally stiff wings. For a joined-wing airplane, this association is not so clear. The optimized joined-wing structural load paths will be shown to follow the inboard wing leading and trailing edges as evidenced by structural buildup shown in Fig. 3b. Clearly, unconventional structural load paths invite unconventional design solutions with a possibility for increased aerodynamic performance. From an aerodynamic perspective, thinner airfoils, perhaps with less transonic aerodynamic drag, are enabled. In addition, there is a possibility to leverage nonlinear structural and aeroelastic synergies to benefit vehicle stability and control.

C. Twist-Actuated Aft Wing

As mentioned, the structural load paths follow the wing leading and trailing edges. To avoid placing control surface cutouts on the major load path, aft wing twist actuators were used in lieu of articulated control effectors for pitch trim. The aft wing pivots about a shaft at the wing root. Vehicle trim is controlled in pitch with a torque actuator effecting root twist on the aft wing. Actuation may be realized with pushrods extending up the vertical tail. The twist-actuated wing replaces the function of a trailing-edge flap in conventional wing designs. The aft wing provides ample control authority with minimal drag. Torsional stiffness must be low, and bending stiffness must be high. Torque-compliant structural design that accommodates natural load paths may help advance this concept. An unswept aft wing would facilitate this proposed twist-actuated design.

D. Propulsion

Obviously, the choice of propulsion system has a strong influence on the resulting vehicle design. However, the focus of this paper is on aeroelastic design of the joined-wing structure. A particular mode of propulsion was chosen to close the design process in terms of fuel consumption. A turboprop in a pusher (aft) position was selected for this study.

III. Design Environment

A large community of design specialists has developed an appreciation for design environments where systems design requires geometric models to interact with a number of analysis modules for a wide range of design variables (mission, geometric, properties, etc.) and technology-driven components and generating a number of system performance metrics. A number of commercially available design environments compete for business. For this study, we chose to utilize the Adaptive Modeling Language (AML) URL: http://www.technosoft.com/. AML is characterized by users as a LISP-like scripted language that drives compiled object code. AML user objects differ from traditional object code, for example, C++, in that any object member or method is automatically accessible from within any other object of the code. The base AML class incorporates automated dependency tracking on every member property (member variable) through object inheritance. This is accomplished automatically in the source-code interpreter for each property formula. Dependency tracking provides a model that is always up to date with respect to any change. Demand-driven calculations are also incorporated into the base AML class. This feature allows one to invoke many changes before forcing desired consequences. For instance, the mission state, the wing sweep, the airfoil section, and so on can be changed before forcing a subsequent dependent mass calculation. This aspect of AML tremendously facilitated the joined-wing design process. However, it also requires focused thought toward managing the overall process as the design model becomes more extensive. For instance, dependency tracking had to be overridden with respect to a number of key parameters to avoid repetitive extensive calculations or the possibility of an uncontrolled feedback loop.

The joined-wing design environment presented here benefited from native AML objects for geometric entities used for visualization, volumetric calculations, and model sharing (IGES and Para-Solids). The recently developed AML meshing object was not used in this model. Rather, the capability described next was developed.

A. Configuration Design Tool Development

The design model shown in Fig. 1 was decomposed into approximately 25 primary objects that drive a number of specialized methods and functions. At the base geometry level, these include curve object, contour object, and surface object to control native cubic constructs. At the wing level, the airfoil, wing panel, and wing tip objects form the basis for an assembled joined-wing object. The wing-merge object shown in Fig. 4a and reconfigured in Fig. 4b connects the inboard and outboard portions of the wing geometry.

The structural FEM and aerodynamic panel partitioning are based on the contour object, which linearly interpolates a paved mesh between key or template curves. Grid points and structured element

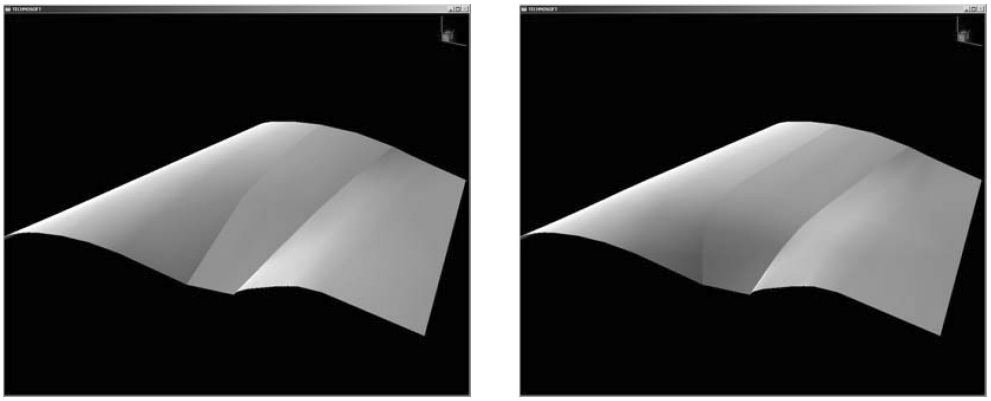

a) b)

Fig. 4 Airfoil variability at wing joint with a) shallow taper and b) steep taper.

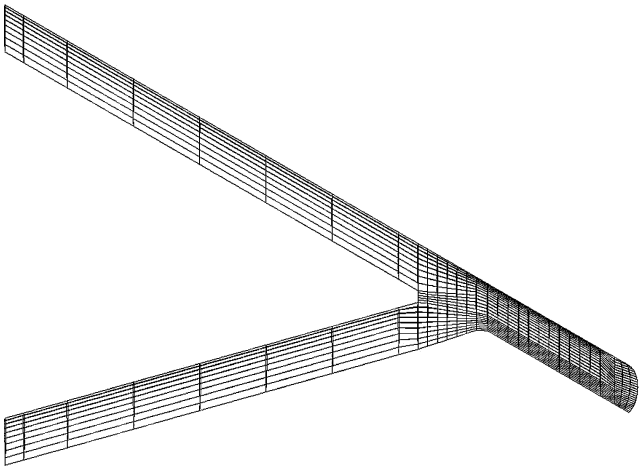

Fig. 5 Web geometry for joined-wing concept with 30-deg tip sweep.

connectivity are tailored to the joined-wing object according to the requested number of rows and columns of elements. The resulting web geometry based on the contour object is shown in Fig 5. Partitioning for structures and aerodynamics models are independently controlled.

Whereas the wing structure and aerodynamic models are consistent with a preliminary level of design detail, the fuselage is not so well defined. For instance, the fuselage mass is parametrically based on textbook formulas and historical regression. Model limitations are addressed hereafter. The fuselage geometry in Fig. 1 does not serve any analysis.

B. Joined-Wing Object

The earlier described collection of objects was developed and combined to create IGES and ParaSolids surface representations for computational fluid dynamics (CFD) calculations, panel definitions to drive PanAir input, and a structural finite element modeler to drive input for structural optimization codes ASTROS and NASTRAN. This joined-wing object was based on a very limited airfoil library and was interactively controlled with numerous properties, including scaleable (thickness and chord) airfoils at key locations, twist at key locations, fore–aft wing separation, component sweep and dihedral, taper, and chord.

The following description gives a sense of the level of detail incorporated into this model. The shape of the wing tip scales automatically or can be easily crafted to form a variety of shapes such as a crescent wing. Airfoil blending in the joint (merge) region can be controlled with a single factor. This geometric model assumes that the chord bounding the inboard merge region between the fore and aft wings is constrained to a sharp edge. The bluntness of the edge is variable and is controllable to the limited extent shown in Figs. 4a and 4b. Without detailed aerodynamic modeling, intuition led to the surface shown in Fig. 4b to smooth the wing for less drag.

When the joined-wing vehicle design model was exercised, an extensive amount of work required to complete just one design configuration. Therefore, only one configuration is presented in this paper. Ongoing configuration studies will be reported in a future paper.

IV. Physics-Based Modeling

A. Mass Modeling

The predicted vehicle takeoff mass comprises FEM-based wing structure, parametric fuselage structure mass, tail structure, parametric engine mass, payload, and fuel. The parametric quantities are a function of the gross takeoff mass (GTOM); thus, the parametric calculations were part of a convergence process along with fuel mass calculations. During the dependency-tracking process, the fuselage and tail masses were kept constant following the initial converged baseline calculation. The fuel mass varied with the change in structural mass, and the engine mass was updated with the GTOM.

B. FEM-Based Wing Structure Mass

Wing structural mass comprises skin and substructure FEM element masses. The substructure was densely populated with ribs and spars to discover where the optimized structural material would distribute itself within the substructure. The substructure minimum gauge was allowed to approach small values during the FSD process to identify the unnecessary substructure. Assuming stress-critical design (ignoring buckling, cost, etc.), one expects that the resulting mass will be representative of production substructure, regardless of the number of stress-optimized substructural elements. For instance, a two-spar wing design carries the same bending shear stress as a four-spar wing with one-half of the spar thickness.

C. Fuselage Structural Mass

Nicolai[11] published a parametric formula for fuselage weights of military and commercial transport aircraft,

$$W_F = 4.003(q)^{0.283}(W_{\text{to}})^{0.95}(L/H)^{0.71} \tag{2}$$

where W is the fuselage weight in pounds, q is the maximum dynamic pressure in pounds per square foot, W_{to} is gross takeoff weight in pounds, and L/H is fuselage fineness.

D. Engine Mass

Torenbeek[12] estimates uninstalled turboprop engine weight W_{UE} to fall between 0.35 and 0.55 lb/hp. The joined-wing model assumed 0.45 lb/hp. Constant L/D was assumed as 24. Power is drag times velocity, and velocity is prescribed for a specified Mach and altitude.

Raymer[13] estimates the installed engine weight W_{IE} with the formula

$$W_{IE} = 2.575 W_{UE}^{0.922} \tag{3}$$

E. Fuel Mass

Fuel is carried in the wing and fuselage. Available fuel volume was a constraint, calculated using the tessellated wing surface model. The simple fuel management system distributes the fuel evenly throughout the wing for load alleviation. Managing fuel distribution to minimize trim drag was not part of the process reported here, but is recommended for future studies. In the design study presented here, the vehicle model carries 100 kg of fuel in the fuselage, which is consumed last. The fuel requirement was approximated with the Breguet range equation for level (constant altitude) flight. The mission was partitioned into three (constant altitude) mission segments. The effect of changing altitude is not addressed in any one segment, nor in the transition from one segment to the next. This simplification was justified by the long range and long endurance of the mission. However, future studies would not suffer computationally with higher-fidelity mission profiles.

The Breguet formula is given here in its normal form,

$$R_i = (V/C)(L/D)\,\ell n(M_{i-1}/M_i) \tag{4}$$

where R_i is the range for the ith mission segment, V is velocity, M_{i-1} is the initial mass at the start of a given mission segment, and M_i is the final mass at the end of a given mission segment. For loiter segments with given time and velocity, the equivalent range was calculated.

The joined-wing mass convergence process was initiated by assuming that the empty (no fuel) mass was known and that the GTOM was unknown. The range equation was solved for the fuel requirement over each mission segment, starting with an assumed empty mass. Simultaneously, the fuselage and engine were resized according to their respective parametric formulas. The process was iterated until convergence was achieved to within 1 lb. During the design process, as the wing mass changed, the fuel requirement changed according to the Breguet range equation.

L/D was assumed constant throughout this study, although the capability exists to update L/D with the aerodynamic modeling described subsequently. For this design process, the focus was on optimizing the nonlinear structural model. Future optimization studies should consider both structural weight and L/D as objective functions. For structural analysis, fuel stored in the wing provided inertia relief to counter the aerodynamic load. Following the initial mass sizing, automated dependency tracking assured a consistent mass model with the correct amount of fuel evenly distributed for any point in the mission.

F. Aerodynamic Modeling

The joined-wing design process benefits from a single compressible aerodynamic model to provide loads for structural modeling, drag for an aeroperformance assessment (not employed here), and stability derivatives to establish trimmed flight conditions. Large deformations typical of trimmed HALE concepts are expected to contribute to the physics of the trimmed design. PanAir[14] provides the linear aerodynamic model for large deformations. Drag assessment is based on PanAir sectional lift distribution corrected with two-dimensional airfoil drag data. The drag assessment capability was tested but not incorporated into the process that produced design results. No aerodynamic modeling was applied to the fuselage or vertical tail, even though this can be done in PanAir.

The element partitioning in the joined-wing environment is variable. Panels on the baseline analysis model are shown in Fig. 5. PanAir is a linear aerodynamic solver using the technique of boundary elements, otherwise referred to as aerodynamic paneling. Surface geometry is body fitted with a structured array of quadrilateral panels. The number of panels is a model variable interactively specified by the user. The baseline model contains 1290 elements for the half-wing. Convergence testing was informally approached with the knowledge that the vehicle trim process will always assure the same total load, thus, partially accommodating a less than optimal convergence. Ultimately, there will be a requirement for higher-order aerodynamic modeling.[15] Meanwhile, PanAir is geometrically consistent with the higher-order methods with its body-fitted mesh.

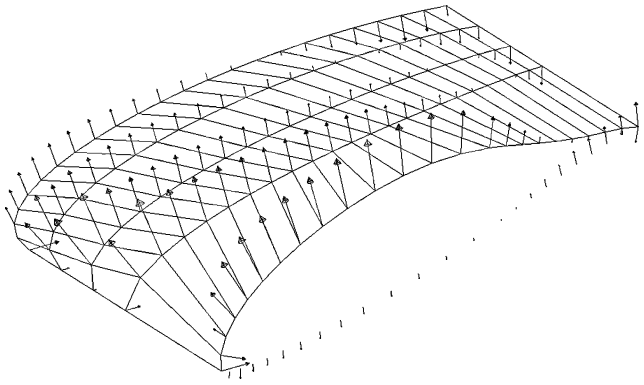

Fig. 6 PanAir pressures on wing tip.

Computer graphics linked with aerodynamic analysis are critical to be sure that the pressures make sense. This is especially true where structural responses are associated with unusual configurations such as the joined wing. Figure 6 shows the wing tip isolated with PanAir pressure vectors depicted at element corner points on the upper surface (and on the lower surface only along the near edge).

Pressures were integrated to determine lift and pitching moment for trim and stability. These integrated quantities were extracted from the PanAir output file. In addition, PanAir provides interpolated pressures at the corners of the panels. These data were extracted from the output and integrated within the joined-wing environment to generate stability derivatives for trim and, more importantly, forces for structural loads. All pressures were applied in the surface normal direction consistent with inviscid flow.

G. Trim and Stability Considerations

System force (z axis) and pitching moment (y axis) were kept in equilibrium with partially automated aerodynamic trim for either the rigid or flexible cases. The trim condition was approached iteratively with a simple Taylor series, based on finite difference approximations to the aerodynamic derivatives. The lift and pitch aerodynamic derivatives were based on a simple linear twist distribution extended over the length of the aft wing from the root to the joint for the rigid case. For the flexible case, the aft wing root twist was imposed in the FEM and the structural solver calculated the flexible aft wing twist. As a result, there was a stress component due to aft wing twist actuation. The deformed condition from the structural analysis included effects of aerodynamic loads plus torque from an actuator that applies the specified twist angle at the aft wing root. This trim process was time consuming and its automation is clearly in order. The process worked with the linear FEM, but ran into difficulties with the nonlinear FEM.

H. Aerodynamic Loads

There was a nominal 5% difference between the lift calculated in PanAir based on constant pressure panels and the externally integrated interpolated pressures. The discrepancy was not explored. However, this difference should not change the results significantly because the loads are fixed to achieve a fixed lift. Therefore, only the distribution of pressure is effected.

I. Drag Buildup

A procedure was developed using tabulated airfoil data generated with XFOIL.[16] XFOIL is a quick response program that couples a two-dimensional panel method with a boundary-layer formulation. The two-dimensional drag data were assumed applicable up to 30 deg of sweep. The procedure calculated a sectional lift coefficient based on PanAir results along each chordwise column of panels. Values of compressible drag coefficient were then interpolated from

the tabulated two-dimensional drag data. Wing drag was the sum of all sectional drag components. This buildup approach approximately accounts for both induced and viscous drag components. The induced drag is accounted for indirectly with angle of attack corrections by matching the sectional lift. The viscous drag is accounted with the boundary-layer theory. Compressibility is implicitly included to the extent possible with Mach-dependent terms included in governing partial differential equations for both PanAir and XFOIL.

Spanwise pressure gradients are not accounted for, and the flow over the bumpy wing joint is clearly in question. The drag buildup used the same tabulated lift and drag data based on a common airfoil shape for the entire wing, including the wing joint. Although this approach is not reliable for accurate prediction of absolute drag (including fuselage and propeller drag, etc.), it is useful in comparing design objective metrics with respect to wing variants.

Although this drag buildup feature is functional and must eventually be included in future design studies, it was not used in this mass convergence. Optimal design convergence is a lengthy process, even with extensive automation, and we chose to forgo a matched drag/fuel/mission loop in the process. Instead, fixed L/D was assumed for the purpose of fuel consumption. Nevertheless, a complete assessment must ultimately include accurate drag accounting.

J. Structural Modeling

All of the work to set up the geometry and the applied loads is preparatory to structural modeling and design. The structural mechanics with indeterminate load paths are complicated even at the most basic, that is, beam structure, level. This is addressed in the following subsection. As will be shown, joined-wing design is dominated by geometrically nonlinear structural mechanics, and a basic description is provided in the next subsection. In the final subsections, the built-up joined-wing FEM model with membrane elements and the optimized solution procedure are described.

The design procedure is a loosely coupled interface between aerodynamic loads calculated by PanAir and structural response to those loads calculated by ASTROS[17] or MSC.NASTRAN.[18] The unique joined-wing configuration employed for a long endurance mission leads to the potential for significant nonlinear structural effects. In the following subsections, how this configuration leads to an unconventional material distribution, what nonlinear structural effects are important, how the structure is modeled, and how the nonlinear analysis was used to determine the material distribution are discussed.

K. Anticipated Structural Load Path

The load path for a joined-wing starts at the wing tip and naturally heads in a direction to achieve a state of least strain energy. Any vertical load will have a component normal to the bending plane (the bending load) and a component parallel to the bending plane. All of the loads considered in this study (taxi, maneuver, gust, and landing impact) are primarily vertical loads of this kind. Consider a pullup maneuver. Bending and in-plane loads are present along the fore and aft wing and pass into the vertical tail and the fuselage. The two paths meet and equilibrate in the fuselage.

Figure 3 shows the plane of minimum bending stiffness by the dotted line connecting the fore–aft wing root. The greatest bending stiffness is obtained by placing material as far from this plane as possible, indicated by the distance d. The dots at the leading and trailing edges indicate where material should be placed in the wing box to obtain a structure with maximum leverage to resist bending. This property of our joined wing suggests that a control surface (or any nonstructural function) not be placed at the trailing or leading edge near either the fore or aft wing roots. Furthermore, we note that the dimension d is driven by the fore–aft wing root vertical and streamwise offsets. Figure 3 indicates that the distance d is greater than the airfoil thickness. Thus, the airfoil thickness-to-chord ratio is not as important to bending stiffness in a joined-wing as it is for a conventional wing. This may increase the freedom to select thinner airfoils without a structural penalty, as Wolkovich suggested.[1]

Wolkovich[1] and Gallman and Kroo[4] reported a forward component in wing tip displacement. The normal to the minimum wing root bending plane points forward. The bending load can be decomposed into normal and tangential components with respect to this plane. The tilted normal component induces a forward component with respect to the vehicle axes. Because the wing bends up and forward, both the aft and front wings have the potential to buckle wherever compression is present.

With those thoughts in mind, there are also the torsional loads to consider, as depicted in Fig. 3b. These torsional loads will contribute significantly to the twisting deformation observed in the nonlinear model. Therefore, torsional stiffness is also an important design parameter.

L. Nonlinear Structures

A HALE uninhabited air vehicle will have very flexible wings due to high aspect ratio for optimal L/D. Therefore, HALE concepts experience large deflections, large enough that the assumption of geometric linearity is violated. Furthermore, the aft wing, which does not exist in conventional aircraft, is especially prone to buckling. Whereas global buckling rarely occurs for conventional aircraft, nonlinear analysis is necessary for highly flexible joined wings. Airframe designers do consider so-called local buckling later during preliminary design. For example, wing skin panels were designed for postbuckling in the design of the C-17 cargo aircraft.

Linear buckling analysis includes only a first-order geometric nonlinearity that leads to an eigenvalue problem that predicts when the structure is unstable. The critical eigenvalue is the magnitude of load for which the deformations may grow unbounded. The higher-order geometric nonlinearity (due to follower forces and certain nonlinear strain terms) may either aggravate or prevent unbounded deformations, but they are ignored in the buckling analysis. The geometrically nonlinear analysis includes the higher-order terms that capture how the structure actually deforms beyond the critical buckling load. In MSC.NASTRAN,[19] the nonlinear stiffness matrix, that is, the tangential stiffness matrix, consists of three parts: the linear stiffness, the geometric (or stress) stiffness, and the stiffness due to large rotation.[19] Buckling eigenanalysis incorporates only the former two. In fully nonlinear analysis, the stiffness due to large, deformation induced rotation is incorporated through the latter matrix, plus an updated Lagrangian approach in which the element coordinate system is updated to the deformed geometry periodically throughout the solution procedure.

M. Structural FEM

Parametrically developed structural meshes for the upper and lower skins were identical. A typical top view is shown with the web geometry in Fig. 5. In addition, the substructure is idealized as a complete "egg crate" of spar and rib plate elements connecting each top plate (QUAD4) element with its lower counterpart. The user may control the number of chordwise and spanwise divisions of the skin. Plate (QUAD4) elements were added at the wingtip leading and trailing edges to facilitate the load transfer from the aerodynamic model to the wing structure. The fuselage and vertical tail were modeled as rigid elements.

N. Structural Solution and FSD Procedure

The skin, spar, and rib elements of the wing box were sized using FSD because traditional, empirical, parametric weight equations are not sufficient for sizing an unconventional joined-wing aircraft. Each time a set of aerodynamic loads was calculated, they were treated as static loads for which the standard NASTRAN[12] procedure was used to converge on geometrically nonlinear equilibrium. The resulting stresses due to flexible, trimmed air loads were used to determine an FSD. Linear material properties were assumed. A factor of safety of 150% was applied to the stress allowable at 100% of the design (maneuver, gust, and impact) loads. The NASTRAN optimizer provides for FSD when linear static analysis is conducted.[18] This procedure was used for the results based on linear analysis. Incorporating buckling would require gradient-based optimization for the wing sizing. This exceeds memory normally available on a desktop personal computer for the many design variables in this application. After the FSD was completed, buckling stability was calculated with NASTRAN.

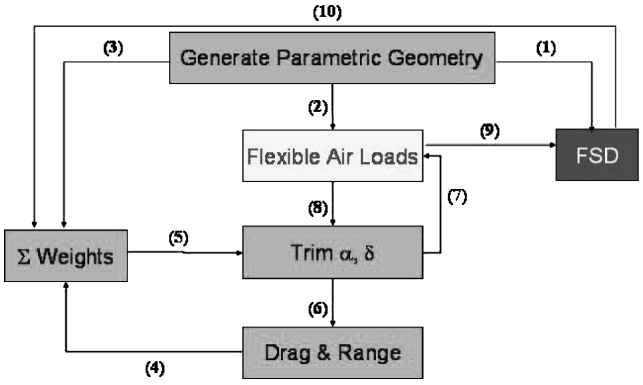

Fig. 7 Design procedure with indices in Table 3.

NASTRAN does not have the capability to perform FSD with a nonlinear structure. Instead, a MATLAB® procedure was developed to carry out FSD with the stresses computed by NASTRAN's nonlinear analysis. The MATLAB program converted the structural model and loads into a NASTRAN nonlinear analysis file.[19] The MATLAB program performed the FSD algorithm to resize each element and create a new NASTRAN input file. For both the linear and nonlinear analysis, the converged FSD was retrimmed using the new aircraft mass and center of gravity until this outer loop of cycles converged on the flexible, trimmed loads (Fig. 7). FSD updates were based on the worst-case stress on each element for all of the impact and nonlinear aeroelastic trimmed load conditions.

Nonlinear analysis on the optimized linear model does not necessarily converge, depending on the postbuckling behavior of the wing. Because optimization of the nonlinear model started with the analysis of a buckling-prone structure, this required some special consideration that is explained here. Whereas a 1.5 safety factor applied to the stress failure condition is equivalent to a 1.5 safety factor applied to the loads for the FSD based on linear analysis, it is not equivalent for nonlinear analysis because stress and load are no longer directly proportional. Applying the safety factor to the stress allowable facilitated the FSD convergence for nonlinear analysis. In other words, the 150% load requirement was exchanged for a 67% stress allowable. This allowed the stress-constrained optimization process to be carried to convergence in the presence of buckling below 150% (and above 100%) of the design load. FSD did not converge when the stress criterion was applied at 150% of the design load. This is discussed in the "FSD Wing Sizing Results" section. Moreover, the additional torsional stresses induced by the flexible aft wing twist exacerbated this convergence problem. Therefore, the flexible aft wing twist was neglected during FSD with nonlinear analysis. This assumption anticipates our development of a twist-compliant aft wing structure that alleviates excessive stress due to twist actuation.

O. Aerostructures Interaction

The solution procedure for converging on nonlinear aeroelastic equilibrium involves a series of corrections starting with rigid loads and ending with flexible loads on a deformed structure. Large deformations require geometrically nonlinear aerodynamic analysis to be addressed. A specialized interface between the aerodynamic panel and structural finite element mesh was programmed in AML. Here, a panel is used to mean the smallest element of partitioning in the PanAir model. Each panel control point (where the tangential flow boundary condition is enforced) is defined internally with respect to the user-specified corner points. The surfaces of the aerodynamic and the structures models are coincident. Therefore, each PanAir corner point falls within a unique structural element on the wing surface. Displacements of corner points in the PanAir model were interpolated from structural grid point displacements of the corresponding structural element. The structural deformation between surface grid points was simply interpolated assuming a flat surface.

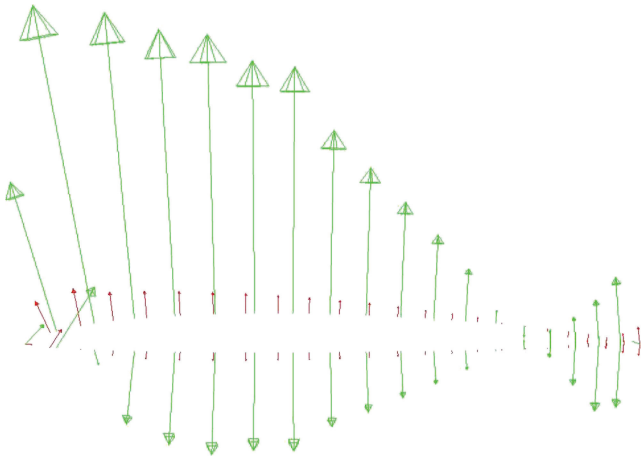

Fig. 8 Aeropressures superimposed over structural forces near the wing tip.

The load transfer process from the aerodynamic model to the FEM was a bit more involved. Each aerodynamic panel was subdivided and the pressure over each panel interpolated based on pressure values at each panel corner of the PanAir model. The integrated normal force at the center of each subpanel was divided and distributed to the four structural grid points of the associated structural element. The allocation was weighted according to the proximity of the normal force to each structural grid, thus maintaining equivalent energy in going from the aerodynamic distribution of pressure to the equivalent structural load at the FEM grid points.

Model validation is always a concern. For instance, it was important to check that the total structural forces equaled the integrated pressure quantities. With respect to distribution, Fig. 8 shows pressure vectors (in red) at points on a section near the wing tip. Structural forces at grid points along the same section of the wing structure are shown in green. This unscaled correlation provides some reassurance that pressures from the aeromodel were properly translated into forces on the structural model.

V. Putting Joined-Wing Design Environment to Work

A. Joined-Wing Design Process

A conceptual design process is a matter of balancing all design considerations until requirements have been met and the system is optimized for cost or performance. Cost and performance are based on either (1) historical regression or (2) manufacturing process and physics-based models. No conceptual regression models exist for joined-wing design. Range and loiter performance can be addressed if one simultaneously knows all of the masses and aerodynamic drag for all segments of the mission profile. The vehicle mass is dominated by fuel and structures. At the detailed structural level, one asks if the vehicle is sufficiently stiff, that is, aeroelastically sound, and strong enough to carry all anticipated loads, for example, balanced maneuver loads and landing loads. The joined-wing designer is quickly confronted with detailed design issues. Clearly, the conceptual and detailed designs are mutually dependent. This joined-wing design process was set up to begin to address this challenge. The two primary design drivers for the joined-wing concept are maximum aerodynamic performance that is, maximum L/D, and minimum structural mass. Structural mass is the focus in the work reported here.

B. Convergence Paths

Nonlinear aeroelastic optimization is an iterative process. The complete overall procedure converges on two objectives: 1) maximized lift/drag and 2) nonlinear structurally minimized mass. The two metrics are mutually dependent through 1) aerostructures interactions, 2) fuel mass, 3) static trim, and 4) mass balancing. Started from a rigid outer surface definition, recursion takes place as follows.

1) Determine aerodynamic performance (L/D) recursion as follows:

a) Integrate pressure into sectional and total lift L components.

b) Obtain sectional drag from tabulated data and sum total drag D.

c) Use new L/D and calculate fuel requirement.

d) Generate new aeroelastic trimmed pressure distribution.

e) Repeat the procedure.

2) Determine nonlinear structurally optimized mass as follows:

a) Convert pressures, fuel masses, and landing loads into FEM force components.

b) Calculate nonlinear structural deformation and stress.

c) Employ FSD for optimal mass.

d) Update aeromesh with deformed structure.

e) Trim deformed FSD with aerosurfaces.

f) Calculate new pressure distribution.

g) Repeat the procedure.

Each new structural design using FSD influences vehicle mass, forcing all of the foregoing to be reconsidered. Convergence on an acceptable design requires multiple iterative processes. Even with the automated processes built into this design model, this overall convergence required more resources than were available for this study. Hence, the current design focused on nonlinear structurally optimized mass for fixed L/D. Note that the overall system design depends on optimized mass and lift/drag together.

C. Structurally Focused Design Process

With user-driven input and automated dependency tracking, many paths were initially available for maneuvering through the design space in the joined-wing design environment. Table 2 provides all of the connectivity that is available (but not necessarily explored at this time) in the joined-wing design environment. Data groups are indexed and listed in the left column. Data processes are listed in the right column with input and output data types. A wide variety of data processes could be extracted from this connectivity. The authors chose a more specific path. Figure 7 and Table 3 comprise the flow diagram for this specific path. To add some sense for this paper, Fig. 7 and Table 3 are somewhat simplified. The basic sequence is indicated in Fig. 7 with numbered arrows, where the data type corresponding to each index is given in Table 3. Figure 7 and Table 3 are useful for explaining the process utilized to converge on the results presented later in this article. Four parallel system analysis elements are involved in the convergence process that leads to a design solution. These elements are outlined here. Each element starts with an "intelligent" assumption that is repeatedly corrected until convergence is achieved.

1) Mission: The lift/drag (L/D) drive fuel weights and subsequently the empty vehicle weight.

2) Loads: The aerodynamic flow is determined by the vehicle shape which is driven in part by component configuration. Other major contributors are vehicle attitude (trim condition) and structural flexibility. Aerodynamic pressures are integrated to form structural loads. Taxi loads are an important non-aerodynamic structural driver.

3) Trim: Static force and moment equilibrium is enforced for the unconstrained symmetric airplane degrees of freedom with input from an aerodynamic control effector. Pitch stability is an important consideration.

4) Structures: The minimum weight structure is driven by material stress allowables and minimum gage, geometrically correct loads, and non-linear structural mechanics. Structural weight recursively influences itself in the presence of gravity.

VI. Design Requirements

System requirements that drive this design process are listed as follows.

1) The required mission (range) includes ingress, loiter, and egress.

2) The Load requirements for structural design include taxi loads (crater impact); a simple pullup maneuver at 2.5 g for start and midpoint of each leg, plus end point of egress; gust at 20,000 ft [Federal Air Regulation Part 23: 60 ft/s ($\Delta\alpha = 4.8$ deg), maneuver 50 ft/s ($\Delta\alpha = 3.5$ deg) at cruise]; and landing loads.

A. Required Mission

This study is roughly based on the published Global Hawk mission profile.[20] The overall design process was simplified by ignoring takeoff, climb, descent, and landing components of the mission, leaving the mission defined in Table 4. An L/D of 24 was assumed to be achievable at Mach 0.6 for ingress and egress. The high Mach number at loiter is required to achieve sufficient dynamic pressure to sustain flight. The propeller specific fuel consumption C_{bhp} was assumed to be 0.55, and propeller efficiency was 0.8.

Table 3 Design procedure indices for Fig. 7

Data index	Data type
1	FEM mesh
2	Aerodynamic mesh
3	Default FEM mass
4	Fuel mass
5	Total mass
6	Vehicle attitude
7	Vehicle attitude
8	Aerodynamic derivatives
9	Aerodynamic forces
10	Optimized FEM mass (update optional)

Table 2 Data connectivity

Data	(data in) Computation (data out)
(1) Mission suite	(1,2,3,4) Breguet fuel assessment (9)
(2) GTOM-mass	(1,2,5) Trim analysis (6)
(3) Best aerodynamic L/D data	(12) Aerodynamic panel generation (8)
(4) Best engine data	(6,8) Aerodynamic solver (7)
(5) Position/velocity	(9,10,16) Mass roll-up (2)
(6) Attitude	(12) Configuration layout (11,14)
(7) Aerodynamic pressure distribution	(7) Drag assessment (3)
(8) Linear aerodynamic model	(11) Structure FEM generation (10)
(9) Fuel mass	(10,13,15,17) Structure optimization (10)
(10) Structural mass model	(9,10,7) Critical loads assessment (13)
(11) Structural configuration	(14) Generate subsystems mass (16)
(12) Outer surface definition	
(13) Structural loads model	
(14) Subsystems configuration	
(15) Structural FEM model	
(16) Subsystems mass model	
(17) Aeroelastic modal interface	
(18) Antenna geometry	

Table 4 Baseline mission and aerodynamic parameters

Mission leg	Range	Duration	Velocity	C (SFC)	Dynamic pressure	W_i / W_{i+1}
Ingress	3000 n mile 5550 km	N/A	0.6 Mach at 50,000 ft, 167 m/s	1.39e−4 (1/s)	2600 Pa	1.23
Loiter	N/A	24 h 8.64e4 s	0.6 Mach 65,000 ft, 167 m/s	1.39e−4 (1/s)	1270 Pa	1.87
Egress	3000 n mile 5550 km	N/A	0.6 Mach 50,000 ft, 167 m/s	1.39e−4 (1/s)	2600 Pa	1.23

Table 5 Load cases

Load	Load type	Mission leg	Leg fraction	Fuel remaining, %
1	2.5-g Pullup	Ingress	0.0	100
2	2.5-g Pullup	Ingress	0.5	85
3	2.5-g Pullup	Loiter	0.0	72
4	2.5-g Pullup	Loiter	0.5	38
5	2.5-g Pullup	Egress	0.0	14
6	2.5-g Pullup	Egress	0.5	7
7	2.5-g Pullup	Egress	0.98	0
8	Gust (maneuver)	Descent	0.6	0
9	Gust (cruise)	Descent	0.6	0
10	Taxi (1.75-g impact)	Takeoff	0.0	100
11	Impact (3.0-g landing)	Landing	0.0	0

B. Required Structural Loads

The structural design is required to meet any relevant load requirement at all points in the mission. These are listed in Table 5. This study was arbitrarily limited to symmetric loads. The 2.5-g pullup maneuver loads were applied at seven points in the mission. Vertical gust loading was superimposed over trimmed 1-g flight with an equivalent angle of attack based on the gust alleviation factor.[13] There are two gust loads indicated as 8 and 9. Load 8 represents a gust encountered at maneuver speed (airspeed at which full and abrupt control inputs may be applied, slightly slower than cruise speed to account for more severe turbulence with vehicle trimmed for cruise). Load 9 represents a gust encountered in normal trimmed cruise.

VII. Baseline Design Model

A. Configuration

The key baseline geometric parameters are listed in Table 1 and shown in Fig. 2. For this study, these parameters remain constant; however, the design environment facilitates configuration design, in which case these parameters can be varied. To put the baseline into perspective, this vehicle's 68-m wingspan is roughly that of a Boeing 747. The wingspan on the Global Hawk is 35.4 m.

B. Materials

Composite materials prevail in optimized HALE wing designs where minimum gauge and stiffness issues prevail. Other considerations, such as multifunctional structures for load-bearing antennas, will eventually become a design factor that dictate the use of composites. However, composite materials would add unnecessary complexity to this joined-wing design study where basic isotropic material design is not yet established. This additional complexity appears in the form of composite type selections and fiber orientation. The aluminum design will illustrate the process and provide a reasonable target wing mass. Thus, the structural material for this wing design study was (isotropic) aluminum. The allowable von Mises stress was 179 MPa, based on a 1.5 safety factor applied to shear and yield stress allowable of 269 MPa for aluminum. A minimum structural thickness of 0.10 cm (0.040 in.) was imposed.

C. Initial Masses

The initial masses are recorded in Table 6. The payload mass accounts for electronic gear. The wing structural mass was initially estimated at 6780 kg to initiate the fuel estimate. The fixed fuselage mass of 2170 kg was calculated with Eq. (2). Empty takeoff mass (ETOM) and GTOM were calculated in a convergent procedure using the Breguet range equation and parametric nonstructural component mass models. The initial approximate ETOM was 13,700 kg, and GTOM was 38,300 kg. It can be compared to the published Global Hawk[20] ETOM of 11,600 kg (same mission) and the published[21] Boeing 747 ETOM of approximately 180,000 kg (same wing span).

Table 6 System weights for initial mission analysis

Component	Mass, kg
Payload	3,550
Engine	1,760
Fuel	24,674
Wing structure	6,780
Fuselage structure	2,170
Tail structure	100
Total assumed	39,034

Uniform thicknesses were assumed for the initial material distribution, resulting in a wing mass of 6780 kg. Once the FSD structural sizing process was begun, the sized structural mass was used for fuel estimation.

The baseline wing has a volume of 71.7 m^3 to carry a maximum 58,100 kg of JP4 fuel. The range analysis, Eq. (1), calls for 24,674 kg of fuel, which occupies under one-half of the available volume for fuel in the wing. Fuel is carried in the wing and fuselage. Fuel was uniformly distributed in the wing throughout the mission with an additional 100 kg contained in the fuselage. Alternate strategies for fuel distribution that minimize trim drag could be investigated, but were not.

D. Aerodynamic Trim

For the rigid case, the baseline aerodynamic center was at 14.6 m from the forward wing apex. With the default skin thickness of 0.00254 m, the trimmed (pitch only) center of pressure at full fuel was 14.5 m with an aft wing twist of 0 deg. In general, the rigid center of pressure was not significantly affected by the choice of airfoil. Further studies will be required to optimize aerodynamic performance. The aerodynamic center remained close to the center of pressure (and, therefore, the center of mass) throughout the design process. Pitch stability was assumed controllable with automated feedback systems. With parasite drag assumed constant at $C_D = 0.01$, Table 7 provides a range of aerodynamic states between ingress and loiter for the rigid baseline. During the optimization process, a constant L/D of 24 was assumed to avoid additional complications with the convergence process.

VIII. FSD Wing Sizing Result

The joined wing was sized using the FSD approach to assign thickness values to the structural elements in the wing boxes. Mass convergence sequences are presented in Tables 8 and 9 for the linear and the nonlinear structural analyses and with the load conditions listed in Table 5. FSD was terminated once the constraint violation

was less than 0.5%. The outer loop on trimmed, flexible loads was terminated when the structural mass changed less than 1%.

A. FSD Based on Linear Analysis

Table 8 lists the wing structure and total vehicle mass after each NASTRAN optimization. Before the first structural sizing iteration, the payload mass was placed at the location required for static aerodynamic stability. After three FSD optimizations, the wing structure mass redistributed enough to cause the aircraft to lose mass balance. At this point in the convergence process, the payload was moved forward in the fuselage to provide a better center of gravity for the remainder of the convergence process. The gust loads were the most critical. When they were neglected, the optimized mass was approximately 2400 kg less than shown in Table 8.

The upper and lower wing skin thickness distributions obtained by FSD using linear analysis are qualitatively the same as the optimized thickness for FSD using nonlinear analysis. Consistent with Ref. 1, the structural mass becomes concentrated at the upper leading edge and lower trailing edge of the fore and aft wing boxes. In the substructure in the aft wing, the aftmost spar increased in thickness as well. Both the trailing-edge skins and spar carry spanwise load. The remaining skin and substructure maintained minimum gauge thickness. This material distribution results from FSD using linear analysis for 11 static, flexible load cases without consideration of buckling constraints.

A buckling analysis was performed a posteriori for all optimized load cases. One critical buckling case occurred at 108% of the taxi crater impact load. The most severe buckling for this case occurred in the forward wing, as expected for a download for which the forward wing is in compression. Thus, the taxi condition is critical for a joined wing, when the forward wing might not otherwise be considered buckling critical. All maneuver conditions exhibited critical buckling at 166% of maneuver load or higher.

Critical buckling for the maneuver gust and cruise speed gust conditions, primarily aft wing buckling, occurred at 67 and 75% of the gust load, respectively. The conclusion is that FSD based on linear analysis is insufficient to obtain a buckling-safe design. The results indicate the need for FSD that is based on nonlinear analysis.

Table 7 Rigid trimmed parameters

Parameter	Ingress	Loiter
C_L	0.981	1.15
C_D	0.0403	0.054
L/D	24.3	21.3
Aerodynamic center, m	14.5	14.6
Center of pressure, m	13.3	14.2

Table 8 Optimized mass at structural iterations using linear analysis

Iteration	Wing structure, kg	Fuel mass, kg	Gross mass, kg
0	6780	26,428	41,050
1	6297	25,237	39,198
2	5354	22,900	35,568
3	7634	28,540	44,330
4	7659	28,602	44,426

Table 9 Optimized mass at structural iterations using nonlinear analysis

Iteration	Wing structure, kg	Fuel mass, kg	Gross mass, kg
0	7,659	28,602	44,426
1	10,399	35,346	54,900
2	11,290	37,533	58,297
3	12,075	39,288	61,092
4	13,181	42,164	65,491
5	12,495	40,485	62,883
6	12,627	40,809	63,385

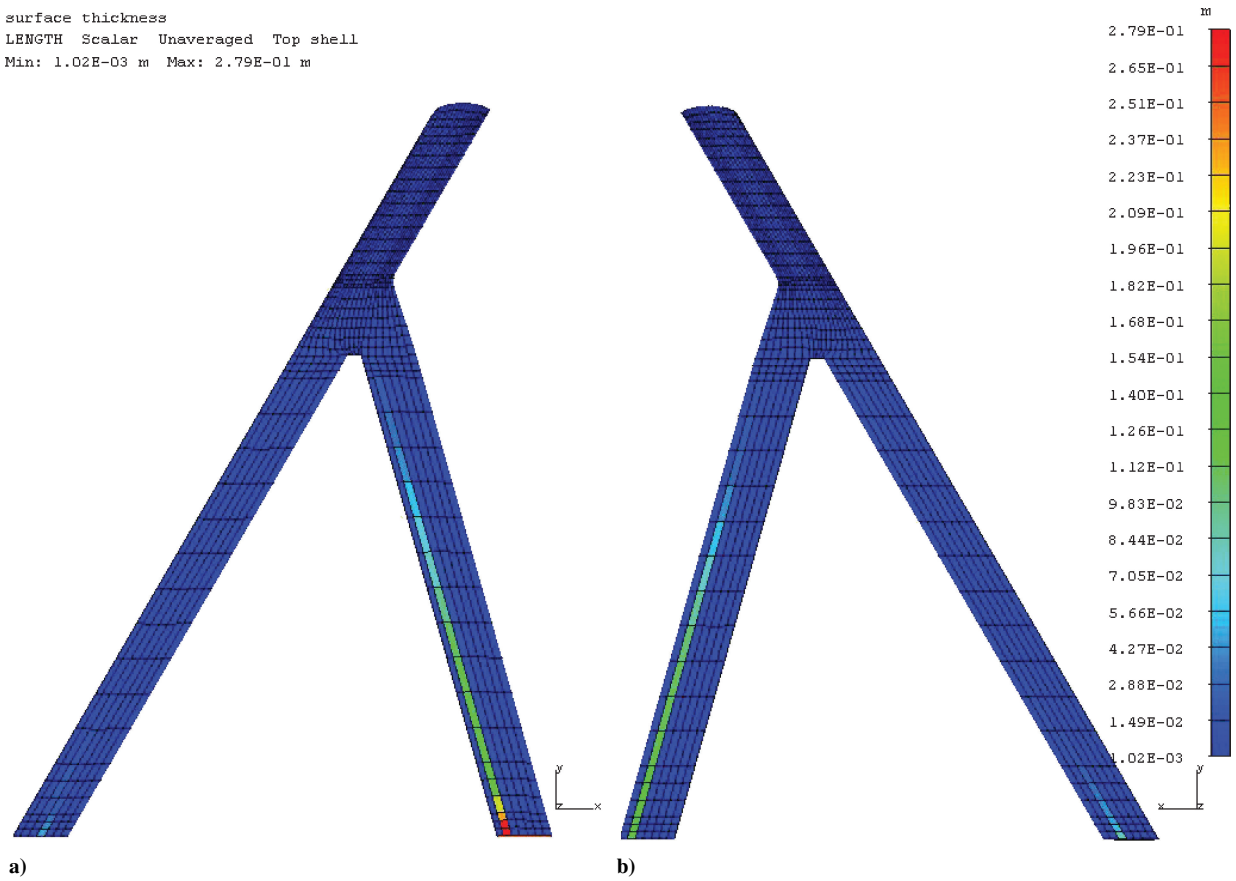

Fig. 9 Skin thickness a) top and b) bottom for FSD by nonlinear analysis.

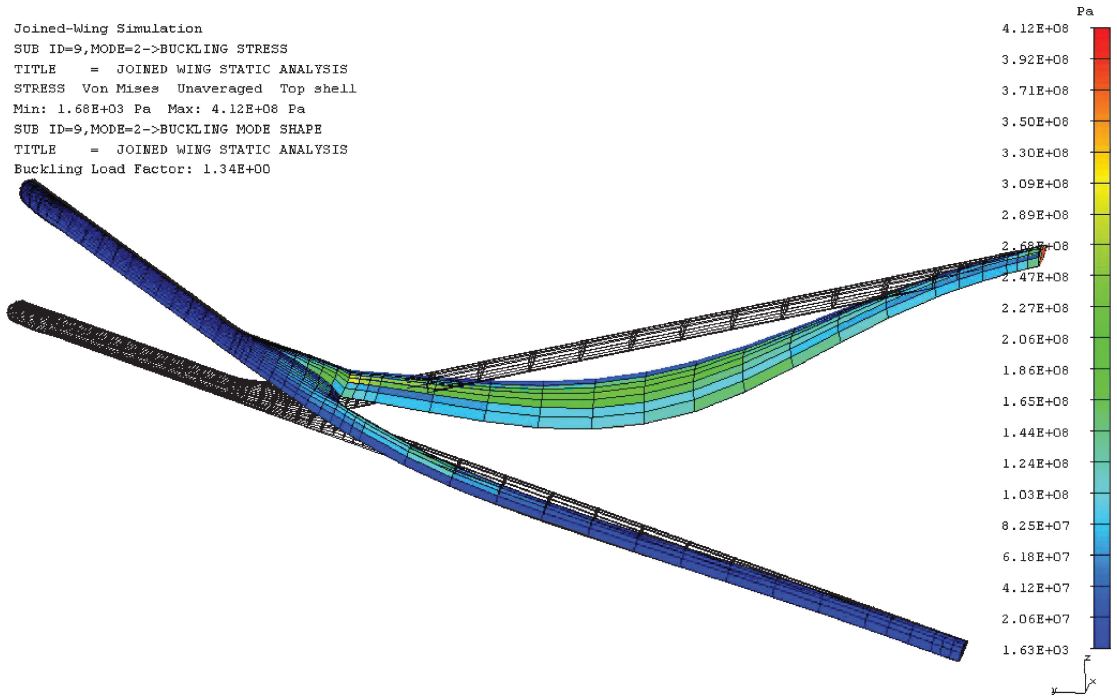

Fig. 10 Buckling mode for gust load for FSD by nonlinear analysis.

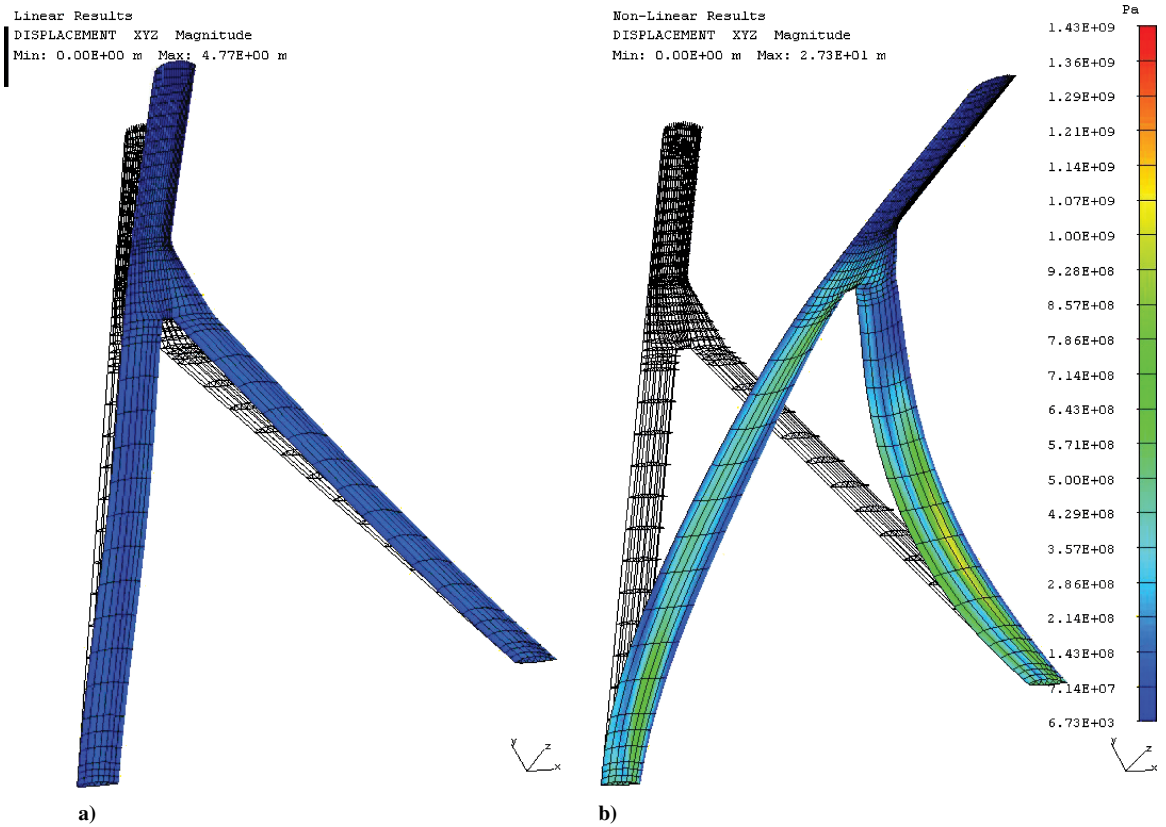

a) **b)**

Fig. 11 Maneuver speed gust analyses of FSD based on linear analysis: a) linear and b) nonlinear.

The buckling mode shape for a gust load applied to FSD linear model is qualitatively the same as for the FSD nonlinear model.

To investigate further the effect of nonlinear structural modeling, the results obtained via FSD based on linear analysis were analyzed next using fully nonlinear analysis. A comparison of the deflections and stress contours in Figs. 11a and 11b demonstrates that the nonlinear response of the aft wing is critical for a viable structural design. The load case is the same for both Figs. 11a and 11b, a gust in a maneuver at 20,000-ft altitude during descent (load case 8 in Table 5). The pressure distribution comes from a combined trimmed 1.0-*G* condition with an additional 4.3-deg gust-induced angle of attack, which constitutes the 100% design gust load factor. However, the load distribution was not the same for the linear and nonlinear analyses because the aeroelastic trim for each case was associated with different deflections. Figure 12 shows the wing tip deflections corresponding to the deformed wing in Fig. 11. The slanted straight line is the linear analysis up to 100% of the maneuver gust load. The wing tip deflection calculated by linear analysis

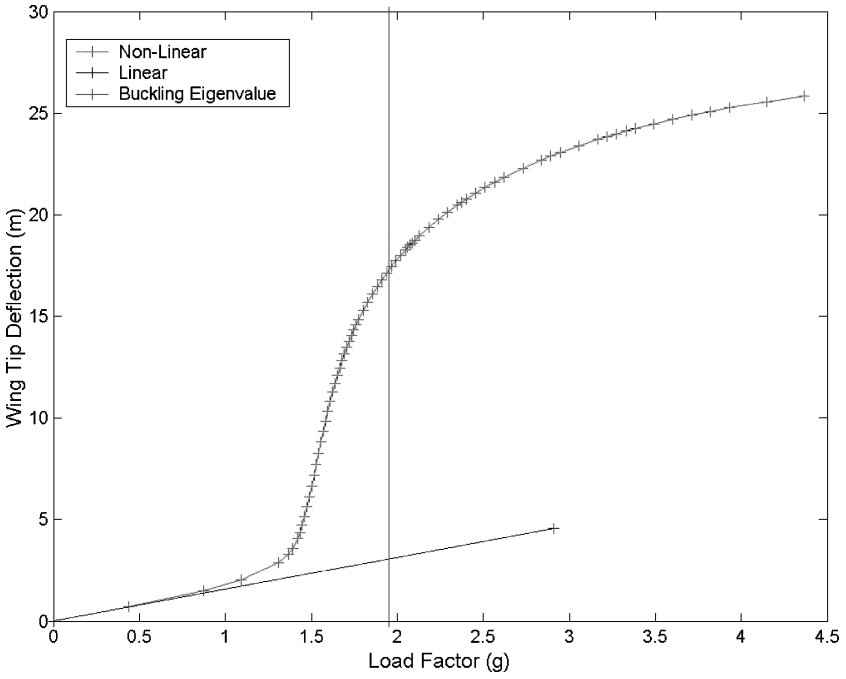

Fig. 12 Wing tip deflection (meters) in nonlinear analysis in Gust.

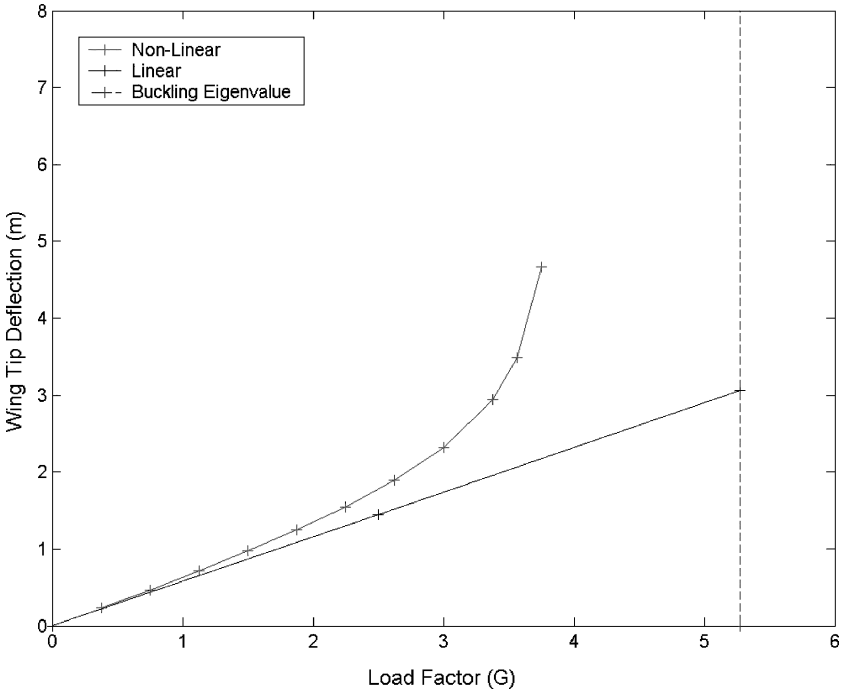

Fig. 13 Wing tip deflection (meters) in nonlinear analysis in 2.5-*G* maneuver.

at 100% of maneuver gust load was 4.77 m (Fig. 11a). The vertical line is the buckling limit, which occurred at 67% of the maneuver gust load. The curved response is the wing tip displacement for nonlinear analysis up to 150% of the design gust load, for which the nonlinear analysis produces a tip deflection of 23.7 m (Fig. 11b).

Figure 13 shows the incremental load vs the wing tip deflection for the 2.5-*G* maneuver load case (load case 1 in Table 5) using linear, buckling, and nonlinear analysis on the FSD based on the linear model. The curved response is the wing tip displacement for nonlinear analysis up to 150% of the design load, that is, a 1.5 factor of safety. The dashed lines represent linear analysis and subsequent buckling. The tip deflection more than doubled in going from linear to nonlinear analysis at 150% of the 2.5-*G* load. The wing tip deflection calculated by linear analysis at 150% of design load was 2.1 m. The buckling load was 211% of the 2.5-*G* load. Obviously, the strains generated by the geometrically nonlinear analysis at this condition would exceed the valid range for the assumption of a linear material. More to the point, the associated stresses far exceed the allowable stress limit. Thus, the nonlinear analysis has proceeded well beyond the failure limit. Both Figs. 12 and 13 indicate that the FSD based on linear analysis is inadequate. For both load cases, it fails, according to buckling analysis and nonlinear analysis.

B. FSD Based on Nonlinear Analysis

The FSD procedure based on stresses from the geometrically nonlinear analysis, described earlier, produced the trimmed and converged optimized masses listed in Table 9. The mass is significantly

heavier than for FSD based on linear analysis given in Table 8, due to the additional material needed to alleviate the violated stresses that had been found in the nonlinear analysis. Figure 9 shows the material distribution on the optimized nonlinear model. The FSD by linear analysis was qualitatively similar, but the nonlinear analysis produced much thicker skins along the leading and trailing edges near the root. This final aluminum design calls for minimum-gauge skins except near the points furthest from the bending plane shown in Fig. 3a. The skin near the aft wing root trailing-edge skin was unreasonably thick, nearly 11 in. thick. The spar thickness remains reasonable: The aft spar of the forward wing reaches 1 in. thick. This effect occurred because no sensitivity information is available to the FSD algorithm to redistribute material to nearby elements when maximum gauge constraints are violated. Clearly, material in these members will need to be redistributed for manufacturing.

The aft wing material was appreciably thicker than on the forward wing (Fig. 9) for several reasons. One is that aft wing buckling was more critical than forward wing buckling for the most severe gust load. Hence, more material was needed to stiffen the aft wing. Also, the aft wing generated lift loads comparable to the forward wing for the optimized configuration. Finally, the component of load that lies in the bending plane acts to place the forward wing in tension and the aft wing in compression. This compounds the compressive load in the aft wing leading edge due to the larger bending load that is normal to the bending plane (Fig. 3b). Conversely, it alleviates somewhat the aft wing trailing-edge tensile load and the forward wing leading-edge compressive load. Thus, the thickest skin elements in Fig. 9 occur in the top surface of the aft wing leading edge.

The deformation of the optimized nonlinear wing is shown in Fig. 14. The load that generates this deformation is listed as load 8 in Table 7, the maneuver gust case. This deformation due to load is qualitatively comparable with the FSD linear model deformation in Fig. 11a. The von Mises stress contours indicate a good distribution of stress, consistent with the premise of a FSD.

Because buckling analysis was not explicitly a part of the FSD procedure, it was checked a posteriori. Once again, the maneuver gust load was the critical buckling load case. The buckled response, that is, the arbitrarily scaled eigenvector, is shown in Fig. 10. The design was buckling safe at design load, that is, FSD at 67% stress allowable, but not to the ultimate load, that is, 1.5 factor of safety. It turned out that critical buckling occurred at only 134% of the maneuver gust (Fig. 15). The wing tip deflection for the final FSD of the nonlinear model shown in Fig. 15 goes unstable shortly after reaching 100% design load, significantly below the 134% buckling condition discussed earlier. (The plus marker on the linear analysis load-deflection line in Fig. 15 indicates a load factor of 2.4 associated with 100% maneuver gust load.) Hence, the structure should be sized to handle stresses from geometrically nonlinear analysis up to the ultimate load to avoid buckling, rather than applying the safety factor to the stress allowable. Alternatively, an explicit buckling constraint could be incorporated; however, the nonlinear deflections in Fig. 14 appear more like the linear analysis in Fig. 11a than the buckling mode in Fig. 10.

A fresh look at the buckling analysis highlighted a negative eigenvalue associated with forward wing buckling and is indicated in Fig. 15. The negative eigenvalue means buckling occurs when the load is reversed. Some component of forward wing buckling can be detected in the nonlinear deflection (Fig. 14), despite the fact that the forward wing buckling mode has a negative eigenvalue. Its effect is perhaps evident in Fig. 15, where the nonlinear analysis becomes unstable as it approaches the (negative) buckling load factor associated with forward wing buckling.

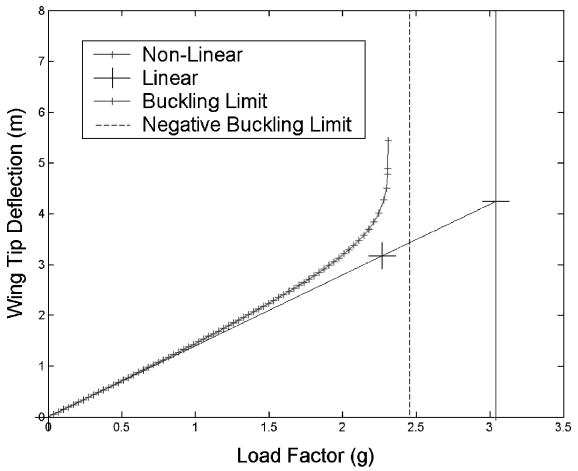

Fig. 15 Load factor vs wing tip deflection of FSD by nonlinear analysis.

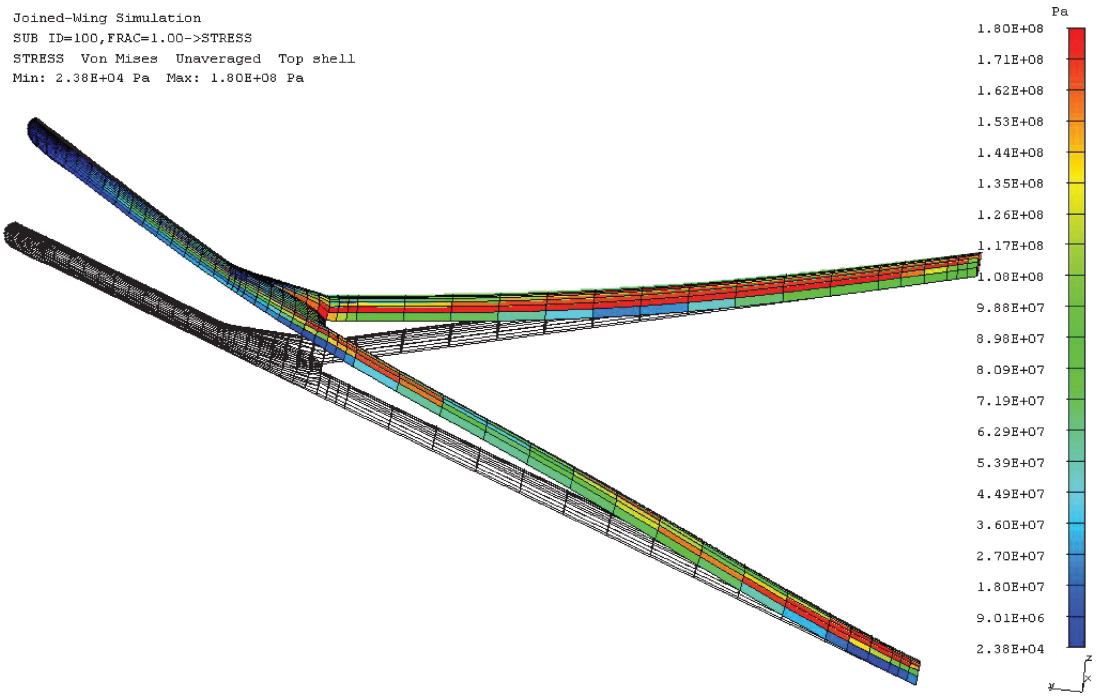

Fig. 14 Deformation with von Mises stress contours for the optimized nonlinear wing.

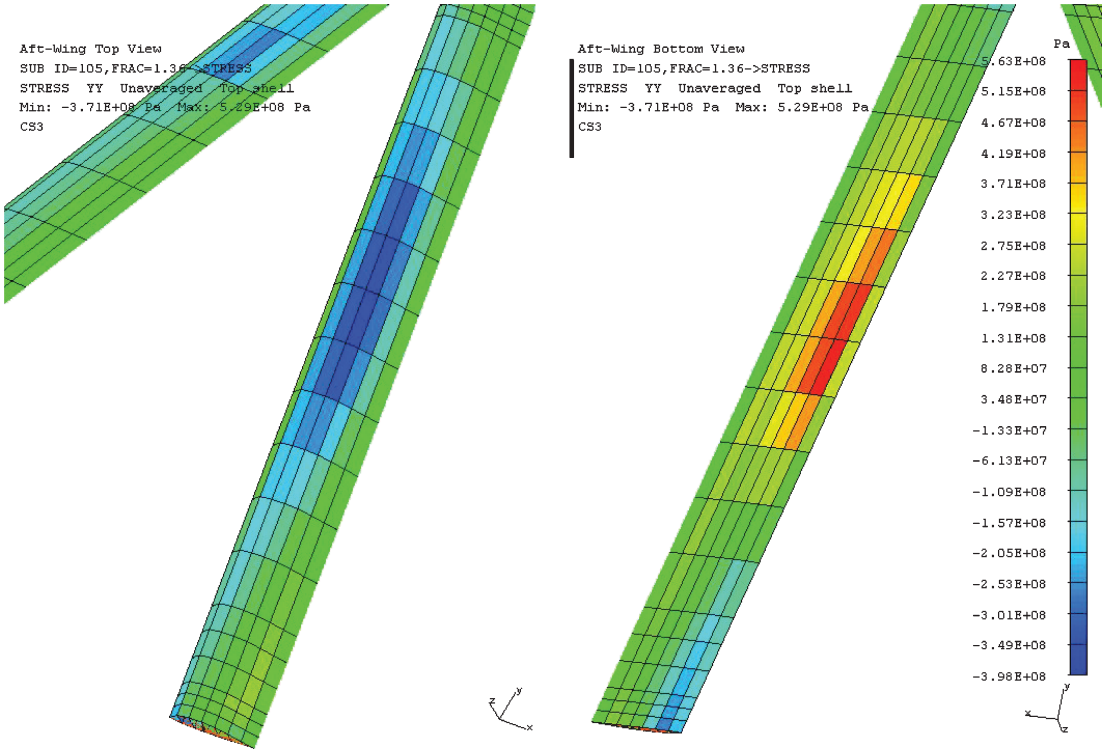

a) b)

Fig. 16 Postbuckled bending stress in aft wing: a) top view and b) bottom view.

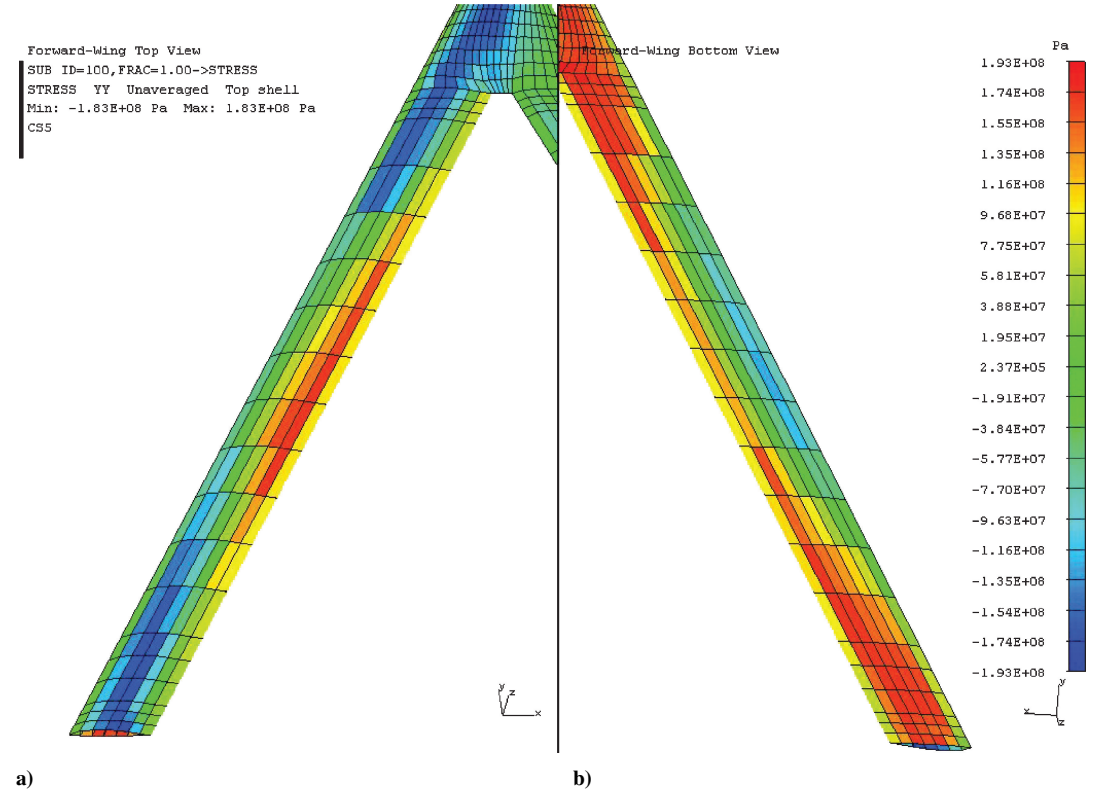

a) b)

Fig. 17 Bending stress in forward wing: a) top view and b) bottom view.

Figure 16 shows the stresses in the aft wing slightly above the 100% maneuver gust load condition indicated in Fig. 15. The high bending stresses in the middle of the aft wing correlates with the curvature in the buckled shape shown in Fig. 10 and indicates that aft wing fails first by rising stresses due to incipient aft wing buckling. The optimization of joined-wing structures will benefit from the integration of FSD with aeroelastically trimmed nonlinear analysis, all in a single convergent procedure.

At the design load, the bending stresses are compressive in the leading edges and tensile in the trailing edges of the forward wing (Fig. 17) and aft wing (Fig. 18). The von Mises stresses in the substructure indicate that the shallow rear spars of the forward and aft wing were the most highly stressed (Fig. 19).

The vehicle trim states calculated during this nonlinear structural convergence procedure are listed in Table 10. We see that the vehicle attitude and pitch trim did not change appreciably during the process.

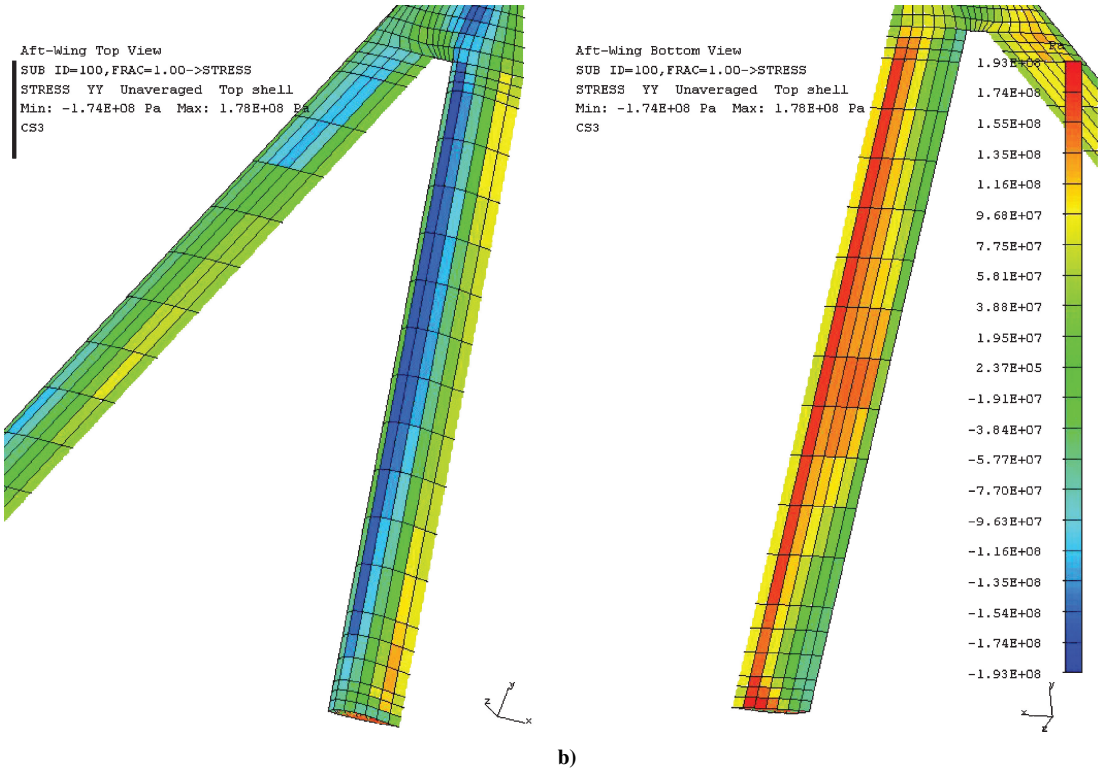

a) b)

Fig. 18 Bending stress in aft wing: a) top view and b) bottom view.

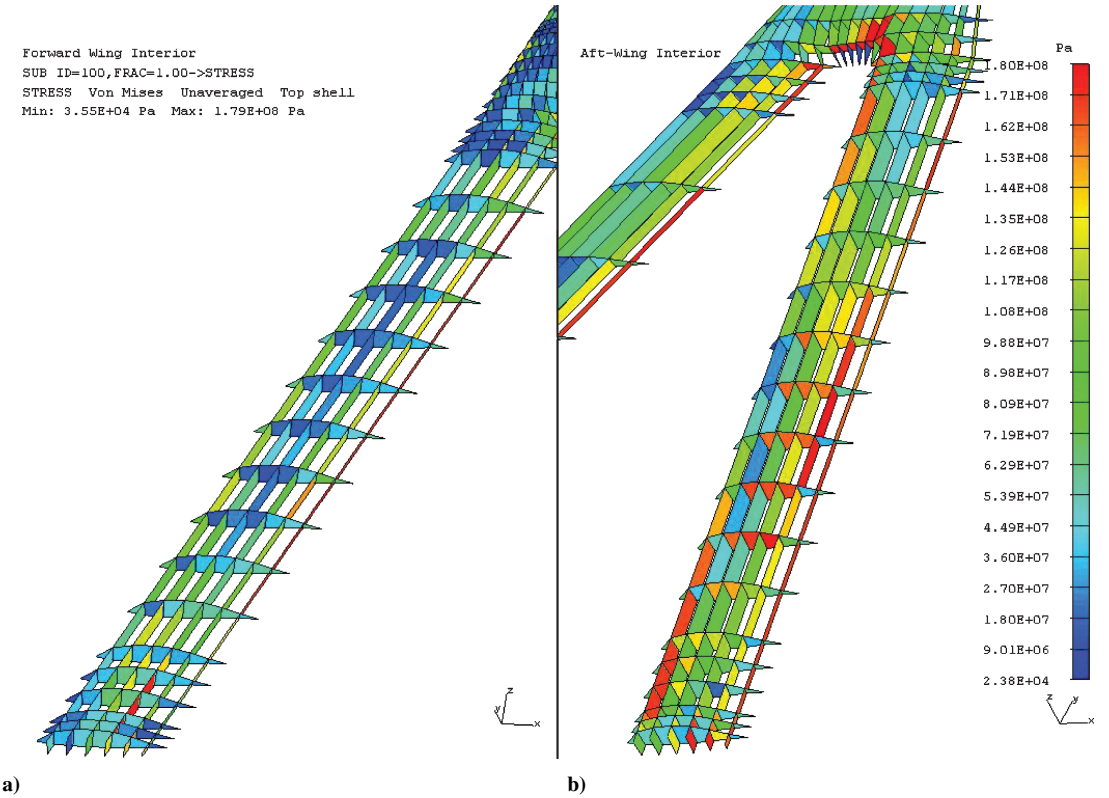

a) b)

Fig. 19 Von Mises stress in substructure: a) forward wing and b) aft wing.

The aerodynamic center, initially ahead of the center of gravity (c.g.), moved aft of the c.g. by the final converged design. Future work will focus more attention on characterizing and optimizing the stability and control of the vehicle.

IX. Discussion

This joined-wing configuration exhibited large geometric nonlinearity below the critical buckling eigenvalue. Thus, nonlinear analysis was required to model correctly this joined-wing configuration.

The gust load with zero fuel proved to be the critical load condition. However, due to the enforced aft wing twist, the stress in the aft wing varies throughout the mission. Thus, it was important to include a wide sampling of mission load cases in the design optimization. The taxi crater impact load condition created large bending stresses in the joined wing. The forward and aft wings

Table 10 Trim history through nonlinear analysis

Iteration	1-g Angle of attack end of mission	Δ Angle of attack maneuver speed gust	Aft-wing twist
1	−3.18	+4.58	−0.86
2	−2.73	+4.66	−1.04
3	−3.03	+4.72	−1.03
4	−3.19	+4.80	−0.26
5	−3.02	+4.75	−0.94
6	−3.04	+4.76	−0.78

were subjected to bending moments opposite of those applied during flight conditions. This loading condition was buckling critical for the optimized linear FSD models and stress critical for the optimized nonlinear FSD model.

FSD and gradient-based optimization for this joined-wing design were expected to result in nearly the same material distribution. (The buckling load was not reached when the stress limit was satisfied in the nonlinear analysis.) However, gradient-based computational requirements would have been prohibitive in this design process without drastically reducing the number of structural sizing variables.

The FSD procedure applied to the geometrically nonlinear structure addresses both strength and buckling. If buckling was encountered, the nonlinear analysis would have likely gone unstable, no equilibrium stresses would be computed, and FSD would have no results to minimize. Fortunately, the nonlinear analysis did not encounter buckling during the convergence process. However, this was only because we replaced the 150% load requirement with a 67% stress allowable. Future design studies should satisfy the ultimate load requirement.

For some trim conditions, the nonlinear (buckling mode) shape tends to unload (washout) the outboard wing tip. This effect might be leveraged or passively induced to create an aeroelastically fail-safe joined-wing design, particularly if the aft wing can be aeroelastically tailored with composite materials to reduce the flexible load increment. If a global, postbuckled response is allowed in the design process, then the washout effect could conceivably create an aerodynamically stable situation. If the wing is designed to withstand the nonlinear stresses, it may be possible to fly in the proximity of the postbuckled state. This would be a major design challenge, ready for intense research.

There was an effort employed to include structural twist actuation in the optimization process for the nonlinear structural model. The design process seemed to go unstable as structural mass was added to carry the applied twist load, which, in turn, required excessive aerodynamic twist to realize a trim condition. In reality, the aft wing will require some compliant mechanism to soften twist stiffness while maintaining bending stiffness. This and other unconventional design approaches are being considered from a research perspective.

The final masses presented here should be kept in a proper context. These masses are not an absolute prediction. For instance, the component masses are taken from published historical regressions based on conventional aircraft. Only isotropic materials were addressed. There was no attempt to address the incorporation of composite materials and the benefits of advanced structural concepts. Consequently, there was no opportunity to employ aeroelastic tailoring and aeroelastic benefits. Furthermore, the grossly redundant substructure was constrained to minimum gauge thickness. Significant design and experimental work remains before a definitive judgment would be possible.

The joined-wing design process employed here was unique in that aeroelastic trim was integrated with FSD for optimal mass design on a nonlinear structures model. Next steps should include drag estimates and fuel management for minimum trim drag. Although significant progress has been made, this joined-wing design procedure is not yet complete for developing mass estimations based on nonlinear aeroelastic design models. Drag was monitored only. It did not enter the range equation because L/D was fixed. Ultimately, high-order CFD should be employed for drag estimation. Contributing challenges include flow over the wing joint and high lift conditions required at extreme altitudes. Also, balanced fuel management will be required to optimize for minimum trim drag.

X. Conclusions

This study demonstrated the ability to converge a structurally optimized and aerodynamically trimmed conceptual joined-wing design. Multiple load cases were required to optimize the model for all expected flight and ground conditions. Aerodynamic stability with respect to the aerodynamic center was not enforced during the resizing process, but was not considered a major hurdle with automated controls. This preliminary study makes the case for optimization of integrated, nonlinear aerodynamic and nonlinear structural problems. Current results demonstrate the need for the nonlinear structural analysis in the design of joined-wing concepts.

The current approach proved to be useful for conceptual design and integrated structural-aerodynamic analysis. The structural buildup preferred the leading and trailing edges for maximum bending about the minimum-bending plane (Figs. 3a and 3b). This conflicts with the placement of trailing-edge control surfaces along the aft wing root and supports the proposed aft wing twist actuation for pitch trim.

Although we are confident in the theoretical integrity of the analysis tools used in this study, we conducted no experimental validation of the nonlinear structural mechanisms rendered in joined-wing configurations. This is highly recommended at this point in time.

A significant amount of engineering programming was completed in AML's LISP-like language for the development of this environment and this study. Still, the design convergence process is currently very time consuming and needs additional automation to facilitate the relationship between high-level parameters, for example, geometric configuration variables and system mass and aerodynamic performance.

Acknowledgments

Support from the U.S. Air Force Office of Scientific Research Program Manager, William Hilbun, and from Dayton Area Graduate Studies Institute director, Elizabeth Downie, is gratefully acknowledged. Technical assistance was also provided by Elizabeth Newsome of Purdue University, Jeremiah Allen of Wright State University, and Jason Robinson of the U.S. Air Force Research Laboratory. Assistance in interpreting results with our PanAir models was provided by Andrew Cary of The Boeing Airplane Company. Ronald Roberts was honored for his contributions with the best thesis award from the Air Force Institute of Technology Department of Aeronautics and Astronautics. The authors are also grateful for the many noteworthy comments offered by the reviewers.

References

[1]Wolkovich, J., "Joined-Wing: An Overview," *Journal of Aircraft*, Vol. 23, No. 3, 1986, pp. 161–178.

[2]Hajela, P., and Chen, J. L., "Preliminary Weight Estimation of Conventional and Joined Wings Using Equivalent Beam Models," *Journal of Aircraft*, Vol. 25, No. 6, 1988, pp. 574–576.

[3]Livne, E., "Aeroelasticity of Joined-Wing Airplane Configurations: Past Work and Future Challenges—A Survey," AIAA Paper 2001-1370, April 2001.

[4]Gallman, J. W., and Kroo, I. M., "Structural Optimization for Joined-Wing Synthesis," *Journal of Aircraft*, Vol. 33, No. 1, 1996, pp. 214–223.

[5]Blair, M., and Canfield, R. A., "A Joined-Wing Structural Weight Modeling Study," AIAA Paper 2002-1337, April 2002.

[6]Roberts, R. W., Jr., Canfield, R. A., and Blair, M., "Sensor-Craft Structural Optimization and Analytical Certification," AIAA Paper 2003-1458, April 2003.

[7]Weisshaar, T. A., and Lee, D. H., "Aeroelastic Tailoring of Joined-Wing Configurations," AIAA Paper 2002-1207, April 2002.

[8]Wakayama, S., "Blended-Wing-Body Optimization Problem Setup," AIAA Paper 2000-4740, Sept. 2000.

[9]Samareh, J. A., and Bhatia, K. G., "A Unified Approach to Modeling MultiDisciplinary Interactions," AIAA Paper 2000-4704, Sept. 2000.

[10]Gern, F. H., Ko, A., Sulaeman, E., Gundlach, J. F., Kapania, R. K., and Haftka, R. T., "Multidisciplinary Design Optimization of a Transonic Commercial Transport with Strut-Braced Wing," *Journal of Aircraft*, Vol. 38, No. 6, 2001, pp. 1006–1014.

[11]Nicolai, L. M., *Fundamentals of Aircraft Design*, METS, Inc., San Jose, CA, 1984.

[12]Torenbeek, E., *Synthesis of Subsonic Airplane Design*, Delft Univ. Press Delft, The Netherlands, and Kluwer Academic, Norwell, MA, 1982, p. 99.

[13]Raymer, D. P., *Aircraft Design: A Conceptual Approach*, 3rd ed., AIAA Education Series, AIAA, Reston, VA, 1999, Chap. 15, p. 476.

[14]Magnus, E., and Epton, M. E., "PAN AIR—A Computer Program for Predicting Subsonic or Supersonic Linear Potential Flows About Arbitrary Configurations Using A Higher Order Panel Method," Vol. 1—Theory Document, NASA CR 3251, 1980.

[15]Hur, J., Beran, P., Huttsell, L., and Snyder, R., "Parametric Mesh Deformation for Sensitivity Analysis and Design of a Joined-Wing Aircraft," AIAA Paper 2004-0116, Jan. 2004.

[16]Drela, M., and Youngren, H., "XFOIL Version 6.94," Massachusetts Inst. of Technology, Cambridge, MA, Dec. 2001, URL: http://cromagnon.stanford.edu/aa200b/handouts/xfoil_tutorial.html.

[17]Neill, D. J., Johnson, E. H., and Canfield, R., "ASTROS: A Multidisciplinary Automated Structural Design Tool," *Journal of Aircraft*, Vol. 27, No. 12, 1990, pp. 1021–1027.

[18]Moore, G. J., *MSC/NASTRAN Design Sensitivity and Optimization User's Guide*, MacNeal Schwendler Corp., Los Angeles, 1994.

[19]Lee, S. H., *MSC.NASTRAN Handbook for Nonlinear Analysis*, Vol. 1, MacNeal Schwendler Corp., Los Angeles, 1992, Chap. 5.

[20]"Global Hawk International Briefing," Northrop Grumman Corp., Rept. 452-AS-3948.ppt 5, Aug. 1999.

[21]*Aerospace Source Book, Aviation Week and Space Technology*, Vol. 158, No. 2, 2003.

[22]Roberts, R. W., "Sensor-Craft Structural Optimization and Analytical Certification," M.S. Thesis, School of Aeronautics and Astronautics Air Force Inst. of Technology, Wright–Patterson AFB, OH, March 2003.